Desalination and Water Treatment
www.deswater.com

doi: 10.1080/19443994.2015.1094677

57 (2016) 18755–18769
August

Taylor & Francis
Taylor & Francis Group

Functionalized copper oxide–zinc oxide nanocomposite: synthesis and genetic programming model of dye adsorption

Niyaz Mohammad Mahmoodi[a,*], Hooman Chamani[b], Hamid-Reza Kariminia[b]

[a]*Department of Environmental Research, Institute for Color Science and Technology, Tehran, Iran, Tel. +98 21 22969771; Fax: +98 21 22947537; emails: mahmoodi@icrc.ac.ir, nm_mahmoodi@aut.ac.ir, nm_mahmoodi@yahoo.com*
[b]*Department of Chemical & Petroleum Engineering, Sharif University of Technology, Tehran, Iran, emails: Chamani.hooman@yahoo.com (H. Chamani), kariminia@sharif.edu (H.-R. Kariminia)*

Received 18 March 2015; Accepted 8 September 2015

ABSTRACT

The functionalized copper oxide–zinc oxide nanocomposite (FCZN) was synthesized and characterized using Fourier transform infrared, scanning electron microscopy, X-ray diffraction, X-ray fluorescence, and BET. Dye removal from aqueous solution was done in a batch system using FCZN as an adsorbent. The effects of adsorbent dosage, initial dye concentration, pH, temperature, and additive salts on dye removal were investigated. Isotherms, kinetics, and thermodynamics of dye adsorption were studied. Equilibrium and kinetic data were fitted by Langmuir isotherm and pseudo-second-order kinetic, respectively. The thermodynamic data showed that dye adsorption was spontaneous, endothermic, and physical reaction. In addition, genetic programming (GP) was applied in order to predict dye removal using an explicit formula. The results of proposed GP models were in close agreement with the experimental data.

Keywords: Nanocomposite synthesis; Dye removal; Genetic programming model; Isotherm; Kinetic; Thermodynamic

1. Introduction

In recent decades, industrial growth and increase in the number of industries associated with color, lead to the increase in water pollution. Currently, there are lots of industries dealing with dyes such as leather, paper, plastic, textile, food processing, printing, cosmetics, pharmaceutical, and dye manufacturing industry [1,2] and the effluents of these industries are of serious concern because of their adverse effects [3,4]. The dye-containing wastewater can affect the aquatic environment by reducing photosynthetic activity due to the decreased sunlight penetration. In addition, some dyes can cause health problems such as mutation and cancer [5,6]. On the other hand, shortage of drinking water is a critical issue. For these reasons, dye-containing wastewater treatment should be taken seriously. Therefore, various methods have been applied for dye removal from effluents such as membrane filtration, flocculation, coagulation, ozonation, bioelectrochemical system, anaerobic decolorization, [7–13], etc. Simplicity of design, low cost, availability and ability to treat dyes in more concentrated form, are some advantages that make adsorption a suitable choice for dye removal [14,15]. Also, adsorption benefits from some other advantages such as high capacity

*Corresponding author.

and large scale [16]. However, the limitations of this method such as the need to centrifuge should be considered and studied more.

So far different materials have been used as adsorbent, e.g. Wood, Eucalyptus bark, Red mud, Modified sepiolite and zeolite, Calcined alunite, Biosorbent (*Canola hull*), Poly (cyclotriphosphazene-co-4,4-sulfonyldiphenol) [14,17–22]. The studies continue to prepare adsorbent with higher capacity in order to reduce adsorbent dosage and consequently decrease the value of disposal material.

Metal-based nanoparticles have some properties including high ordered structure, high mechanical and thermal strength, high number of vacant reactive surface sites, metallic or semi-metallic behavior, and high surface area which make them applicable for removal of toxic materials [23,24]. Besides, an emerging field in adsorption process is surface functionalization that increases adsorption capacity to a large extent. Table 1 presents dye removal ability of different adsorbents containing metal [25–32].

Also, various methods of modeling have been used in capturing the non-linear relationship existing among variables in complex systems in the field of adsorption process, e.g. neural network [33–35] which is a powerful tool for prediction, but it is not usually able to produce practical prediction equations [36]. Adaptive neuro-fuzzy inference system [37–40] and least square support vector machine [41,42] are some other methods of modeling that were used in this field. However, no reported work was found to use genetic programming (GP) approach for modeling of dye removal in the field of adsorption process. The main advantage of this kind of modeling is to present an explicit formula for prediction.

A literature review showed that dye removal using FCZN was not investigated. Since the synthesized copper oxide–zinc oxide nanocomposite (CZN) had a hierarchical 3D morphology composed of flower-like ZnO microstructure integrated with CuO nanopatches [43], the aim of this study was to investigate the effect of functionalization on the mentioned surface. In this research, CZN was synthesized and functionalized using 3-aminopropyltrimethoxysilane. FCZN was characterized using Fourier transform infrared (FTIR), scanning electron microscopy (SEM), X-ray diffraction (XRD), X-ray fluorescence (XRF), and BET. Three azo dyes (DR23: Direct Red 23, DR80: Direct Red 80 and DR81: Direct Red 80) were used. The reason of selecting these dyes was that more than 60% of dyes used in industries are azo dyes and most of them are non-biodegradable [44,45]. The effects of adsorbent dosage, initial dye concentration, pH, temperature, and additive salts on dye removal were investigated. Isotherms, kinetics, and thermodynamics of dye adsorption were studied. Furthermore, GP was applied for dye adsorption modeling.

2. Materials and methods

2.1. Chemicals

DR23, DR80, and DR81 were purchased from Ciba (Germany) and applied without any purification. The other materials were obtained from Merck.

2.2. Synthesis of FCZN

NaOH (1 g) was dissolved in 90 mL distilled water. $ZnCl_2$ (1 g) was then added to sodium hydroxide solution and stirred for 30 min. In the next step,

Table 1
Dye removal ability of different adsorbents containing metal

Adsorbent	Dye	Q_0 (mg/g)	Refs.
Magnetic Fe_3O_4@graphene nanocomposite	Methylene blue	45	[25]
	Congo red	34	
MnO–Fe_2O_3 composite	Acid red B	105	[26]
MgO nanoparticles	Reactive blue 19	167	[27]
	Reactive red 198	123	
NiO nanoparticle	Congo red	40	[28]
γ-Fe_2O_3	Acridine orange	59	[29]
Magnetic Fe_3O_4@C nanoparticles	Methylene blue	44	[30]
	Cresol red	11	
Zinc oxide loaded on activated carbon	Malachite green	323	[31]
Fe_3O_4 hollow nanospheres	Neutral red	105	[32]
FCZN	Direct red 23	362	[This study]
	Direct red 80	208	
	Direct red 81	160	

$CuSO_4{\cdot}5H_2O$ (1 g) was added and the solution was stirred in the environment temperature for 30 min. The prepared solution was heated in a closed bottle at 100°C for 24 h. The upper liquid was decanted, the solid material was washed three times and then heated to be dried. The dried material was powdered (CZN). For functionalization, CZN (1 g) was added to 1 mL distilled water. Then, 2 mL 3-aminopropyltrimethoxysilane and 20 mL ethanol (96% volumetric) were poured into the solution. The solution was stirred in a closed bottle at environment temperature for 24 h, and then heated at 90°C for 24 h. Fig. 1 shows the mechanism of functionalization. The solid material was powdered (FCZN) and used for further investigation.

2.3. Characterization of FCZN

To determine the point of zero charge (pH_{pzc}) of FCZN, 10 bottles of water (100 mL) with various pH from 2 to 11 were prepared. 0.1 g adsorbent was then added to each bottle and stirred for 24 h [46,47]. By plotting final pH of solution against initial pH, pH_{pzc} was determined as pH 7.

The functional groups of materials were investigated using FTIR spectroscopy (Perkin–Elmer Spectrophotometer Spectrum One) in the range 4,000–450 cm^{-1}. The morphological structure of the FCZN was examined by SEM using LEO 1455VP scanning microscope. The XRD pattern of materials were achieved using a D8 ADVANCE XRD spectrometer (Bruker, German) with a Cu Kα target at 40 kV and 50 mA at a scan rate of 0.02° 2θ s^{-1}. The XRF analysis was performed on ARL 8410 to obtain the chemical composition of the samples. Brunauer–Emmett–Teller (BET) surface analyzer (Micromeritics 3020, USA) was employed to study the surface anatomical properties.

2.4. Dye adsorption

Batch adsorption experiments were performed by mixing the adsorbent with 250 mL of dye solution for 60 min. Each experiment was sampled at specific time intervals (0, 2.5, 5, 7.5, 10, 15, 20, 30, 40, 50, and 60 min). All samples were centrifuged and then the residual dye in the samples was determined using spectrophotometer (Perkin–Elmer Lambda 25) at maximum wavelength (λ_{max}). The values of λ_{max} were 500, 540, and 509 nm for DR23, DR80, and DR81, respectively.

The isotherms and kinetics of adsorption process were investigated using the data obtained from the evaluation of adsorbent dosage and initial dye concentration effect, respectively. Thermodynamics were studied through the data obtained from the study of temperature effect.

2.5. Desorption studies

The FCZN was used for dye adsorption for 60 min (initial concentration = 50 mg/L, pH 2, temperature = 20°C). In the next step, pH of solution was reached to 12 by adding NaOH. The solution was agitated for 60 min. The adsorbed and desorbed dye was determined using first and second step, respectively. The residual dye of each step was determined using spectrophotometer after centrifuging.

3. Result and discussion

3.1. Characterization

The FT-IR spectrum of CZN has two peaks at 3,453 and 497 cm^{-1} (and 615 cm^{-1}) which indicate O–H stretching vibration and metal-oxygen vibration,

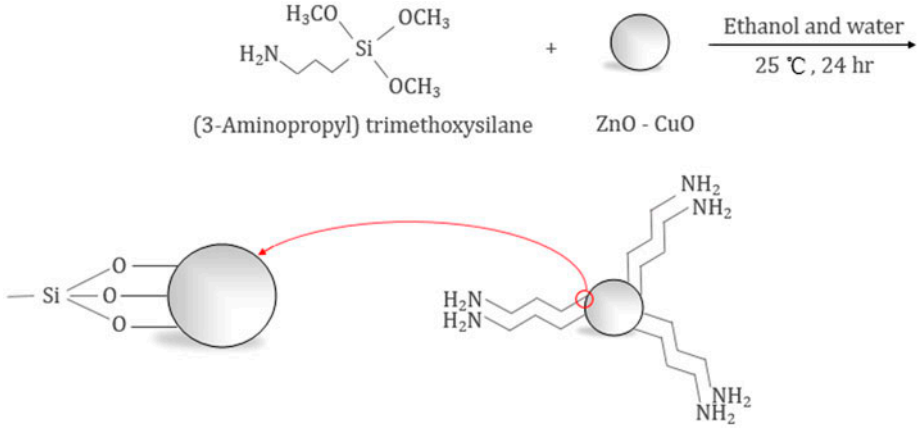

Fig. 1. The mechanism of CZN functionalization.

respectively (Fig. 2). The FTIR spectrum of the FCZN displays a number of characteristic bands at 3,429, 2,944, and 497 cm^{-1} (and 615 cm^{-1}) (Fig. 2). These bands are assigned to O–H and N–H stretching vibration, $–CH_2–$ asymmetric vibration, and metal-oxygen vibration, respectively [48]. The N–H (amine) and C–N (amine) bending vibrations display a strong band at 1,600–1,560 cm^{-1} and 1,350–1,000 cm^{-1}, respectively [48].

SEM has been a primary tool for determining the particle shape, porosity, and appropriate size distribution of the adsorbent. SEM images of FCZN are shown in Fig. 3. It is clear that FCZN is a nanoparticle.

Fig. 4 shows the XRD of CZN. Diffraction peaks are in good agreement with those of the standard patterns of hexagonal wurtzite ZnO (JCPDS Card No. 36-1451) and monoclinic CuO (JCPDS Card No. 05-0661). In Fig. 4, there are two sets of diffraction peaks for the zinc oxide/copper oxide nanocomposite sample, which are correspondingly ascribed to hexagonal wurtzite ZnO and monoclinic CuO, and no peaks of other phases and impurities were detected [43]. Also, after functionalization of CZN, analysis was performed and no change was observed.

The chemical composition of FCZN was determined using XRF. Based on XRF analysis, FCZN has higher ZnO (56%) and lower CuO (34%). In addition, FCZN has 2.6% SiO_2 and 7.4% of the initial weight was lost due to heating the sample at 900˚C for 1 h. The N_2/77 K adsorption isotherm provides useful information about surface anatomical properties. Table 2 shows a summary report of surface area, pore volume, and pore size.

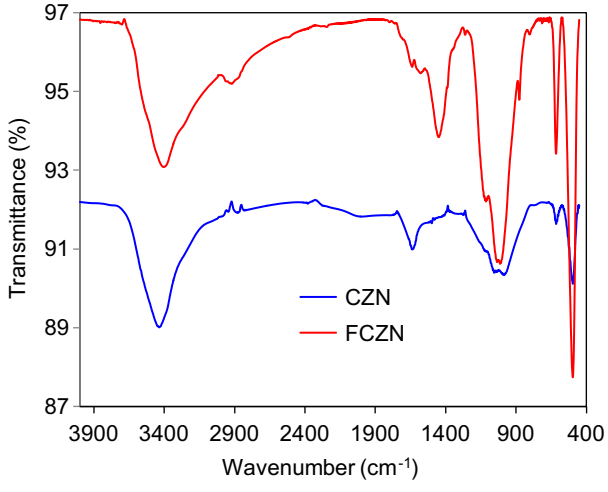

Fig. 2. FT-IR spectrum of CZN and FCZN.

3.2. Effects of operational parameters

3.2.1. Effect of adsorbent dosage

By conducting experiments at a similar condition and different adsorbent dosage range of 0.025–0.15 g/L for DR23, 0.08–0.26 g/L for DR80, and 0.05–0.3 g/L for DR81, the effect of adsorbent dosage on dye adsorption was investigated. Figs. 5 and 6 illustrate the results for CZN and FCZN, respectively. According to these figures, the adsorption capacity of FCZN was much better than CZN. It can be attributed to the presence of amine functional group of FCZN. At acidic pH, amine group ($–NH_2$) of FCZN is converted to positively charged group ($–NH_3^+$). A significantly high electrostatic attraction exists between the positively charged surface of the adsorbent, due to the ionization of functional groups of adsorbent and negatively charged anionic dye. Since FCZN took precedence over CZN in terms of the values of dye removal percent, FCZN was used for further studies.

Increasing the amount of adsorbent increases the available and suitable sites on the adsorbent surface, and consequently leads to the increase in the dye removal percent. However, the adsorption capacity (mg adsorbed dye per g adsorbent) is reduced. It can be related to overlapping or aggregation of adsorption sites resulting in a decrease in total adsorbent surface area available to the dye and an increase in diffusion path length [49,50].

3.2.2. Effect of initial dye concentration

The effect of initial dye concentration on dye removal was studied in the initial dye concentration range of 50–200 mg/L. Fig. 7 shows the effect of initial dye concentration on dye removal using FCZN. It can be seen that the higher the initial concentration, the lower the percent of dye removal. At a constant adsorbent dosage, the decrease in the adsorption percent is probably due to the saturation of the active binding sites on the FCZN surface at higher dye concentrations. However, if the amount of adsorbent is kept unchanged, increasing the amount of initial dye concentration increases the amount of dye adsorbed onto the adsorbent, due to the increase in the driving force of the concentration gradient at the higher initial dye concentration [51].

3.2.3. Effect of pH

The effect of pH on dye adsorption was studied by conducting experiments at a similar condition and different pH in the range of 2–10. Fig. 8 illustrates the

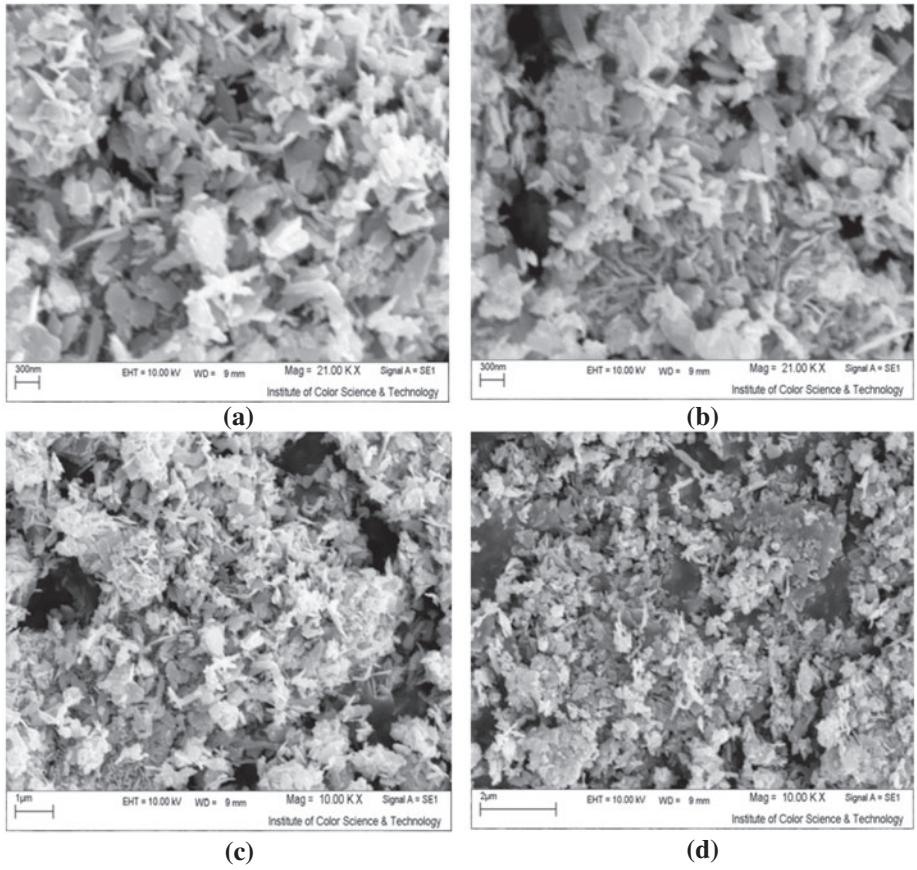

Fig. 3. SEM images of FCZN with different magnifications (a,b) 300 nm, (c) 1 μm, and (d) 2 μm.

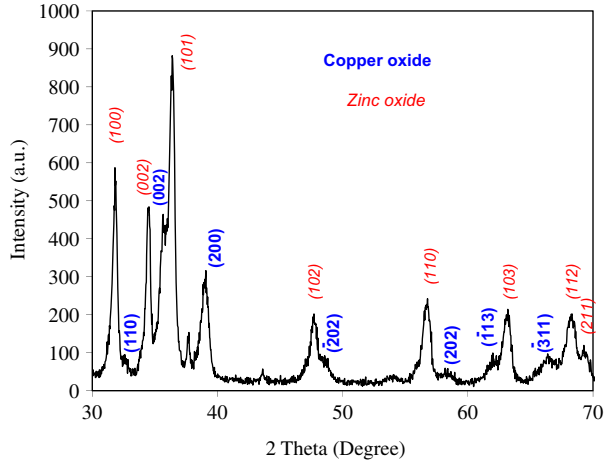

Fig. 4. XRD pattern of CZN.

effect of pH on dye removal. If the pH of the solution is less or more than pH_{pzc}, the adsorbent surface gets positive or negative charge, respectively [52]. The decrease in pH increases the electrostatic interaction between the negatively charged dye molecules and the FCZN surface sites, which favors the uptake of dye anions. As a consequence, the lowest pH (pH 2) in which the adsorbent had more positive charge, was the best pH value for dye removal. On the other hand, presence of excess OH^- at alkaline pH destabilizes anionic dyes and also competes with dyes for achieving empty sites on the adsorbent surface.

3.2.4. Effect of additive salts

NaCl, Na_2SO_4, and $NaNO_3$ were used as additive salts in this investigation. Presence of these salts are common in the wastewater of color industries, e.g. NaCl can be used in textile industry because it has coating effect on surface charge of fiber and improves the connection between the dye and the fiber. Therefore, sodium chloride may be found in industrial effluents. The presence of anions in wastewater can cause two problems: (i) anions and dyes may compete for active sites on the adsorbent surface. (ii) Anions can deactivate the adsorbent surface. Both of these situations can reduce the amount of adsorbed dye.

Table 2
The properties of FCZN

Parameter	Value
Surface area	
Single point surface area at p/p° = 0.222782128	8.2981 m/g
BET surface area	7.9675 m/g
Langmuir surface area	10.7721 m/g
Pore volume	
Single point adsorption total pore volume of pores less than 1,255.659 Å width at p/p° = 0.984339111	0.036023 cm/g
t-plot micropore volume	0.004045 cm/g
BJH adsorption cumulative volume of pores between 17.000 and 3,000.000 Å width	0.049028 cm/g
BJH Desorption cumulative volume of pores between 17.000 and 3,000.000 Å width	0.048974 cm/g
Pore size	
Adsorption average pore width (4 V/A by BET)	180.8504 Å
BJH adsorption average pore width (4 V/A)	464.134 Å
BJH desorption average pore width (4 V/A)	334.748 Å

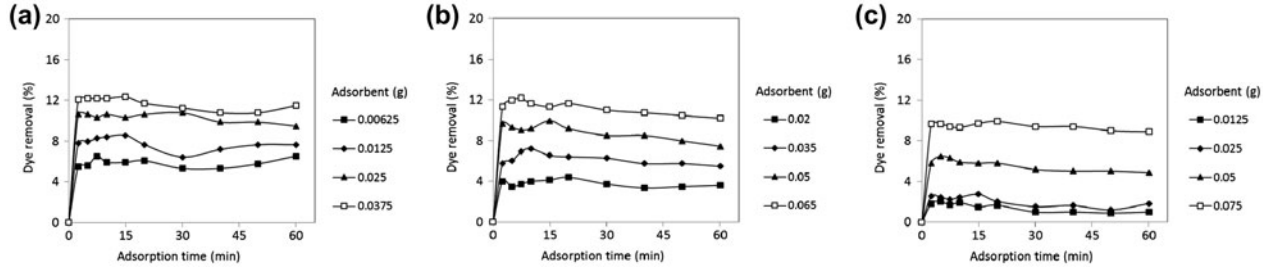

Fig. 5. The effect of adsorbent dosage on dye removal percent using CZN: (a) DR23, (b) DR80, and (c) DR81 (initial concentration = 50 mg/L, pH 2, temperature = 20°C).

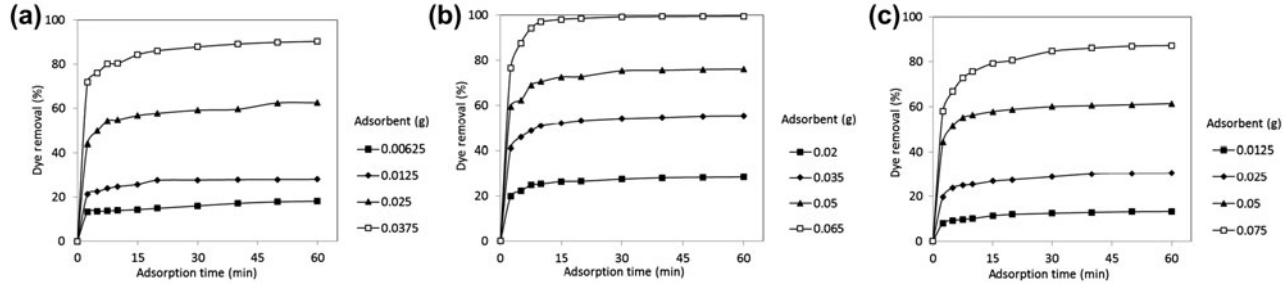

Fig. 6. The effect of adsorbent dosage on dye removal percent using FCZN: (a) DR23, (b) DR80, and (c) DR81 (initial concentration = 50 mg/L, pH 2, temperature = 20°C).

As it can be seen in Fig. 9, adding salts reduced the dye removal percent.

3.2.5. Effect of temperature

The effect of temperature on dye adsorption was investigated at different temperatures in the range of 20–50°C. As shown in Fig. 10, temperature has positive effect on dye removal percent. Increasing temperature enhances the rate of diffusion of the adsorbate molecules across the external boundary layer and in internal pores of adsorbent, owing to the decrease in the viscosity and increase in diffusion coefficient of dye. Furthermore, changing the temperature has effect on the equilibrium capacity of the adsorbent for a particular adsorbate [53,54].

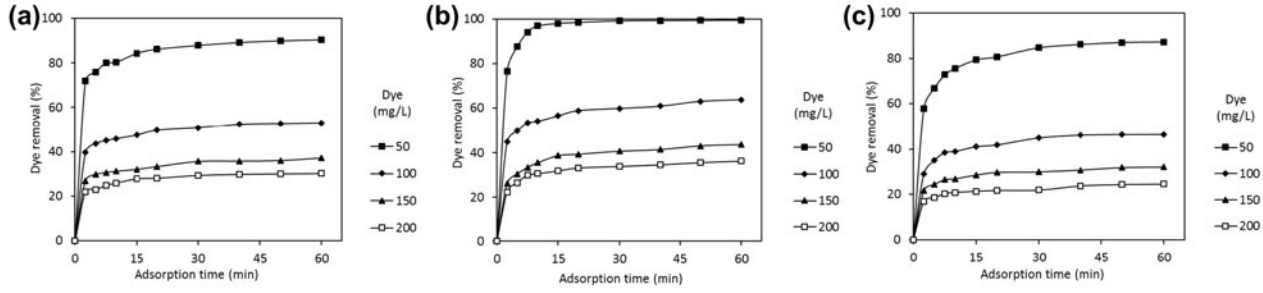

Fig. 7. The effect of initial dye concentration on dye removal percent using FCZN: (a) DR23, (b) DR80, and (c) DR81 (adsorbent dosages were 0.15, 0.26, and 0.3 g/L for DR23, DR80, and DR81, respectively, pH 2, temperature = 20˚C).

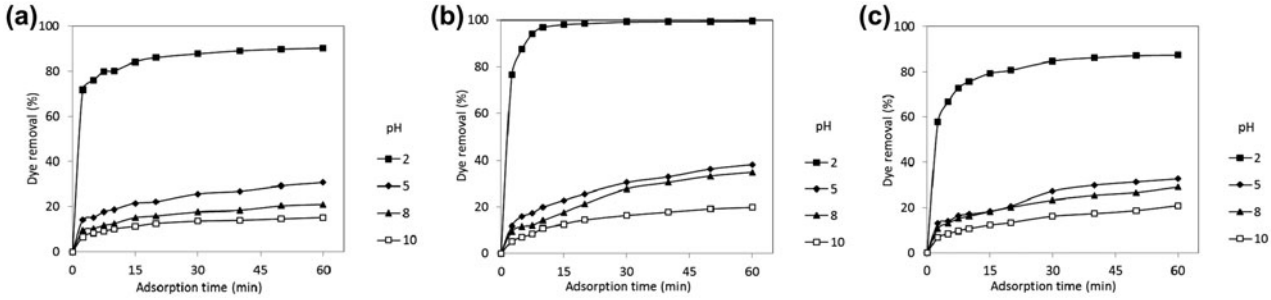

Fig. 8. The effect of pH on dye removal percent using FCZN: (a) DR23, (b) DR80, and (c) DR81 (adsorbent dosages were 0.15, 0.26, and 0.3 g/L for DR23, DR80, and DR81, respectively, initial concentration = 50 mg/L, temperature = 20˚C).

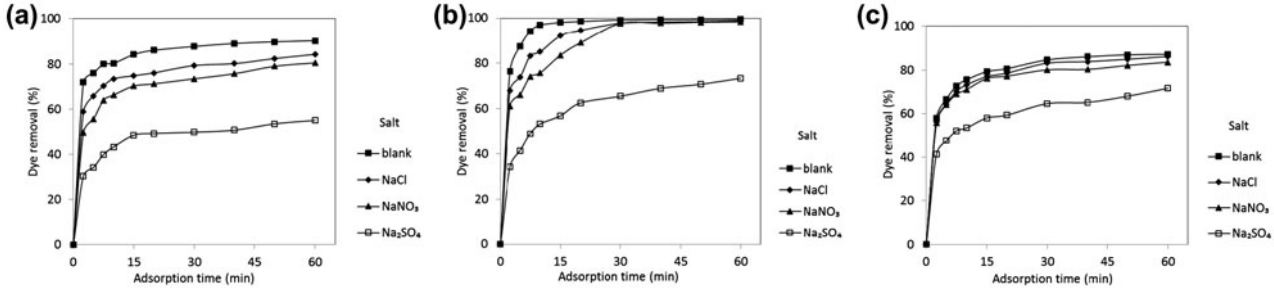

Fig. 9. The effect of additive salts on dye removal percent using FCZN: (a) DR23, (b) DR80, and (c) DR81 (adsorbent dosages were 0.15, 0.26, and 0.3 g/L for DR23, DR80, and DR81, respectively, Initial dye concentration = 50 mg/L, pH 2, temperature = 20˚C, and 0.02 mol/L salt).

3.3. Adsorption isotherm

According to equilibrium data (q_e and C_e), adsorption isotherms describe how molecules of dye and adsorbent surface react with each other. The isotherm plays an important role for designing the adsorption systems. Many isotherm models have been presented for analysis of adsorption process. Langmuir, Freundlich, and Tempkin isotherms are common for solid–liquid systems.

The Langmuir isotherm is based on some assumptions [55]: (i) Adsorption occurs on specific and homogeneous sites within the adsorbent. (ii) Adsorbent has a limited capacity for absorption. (iii) Adsorption sites are identical in terms of energy and structure. (iv) Each site is occupied by a molecule of dye. The Langmuir equation is:

$$q_e = \frac{q_0 K_L C_e}{1 + K_L C_e} \quad (1)$$

where q_e, q_0, C_e, and K_L are the amount of dye adsorbed onto the adsorbent at equilibrium (mg

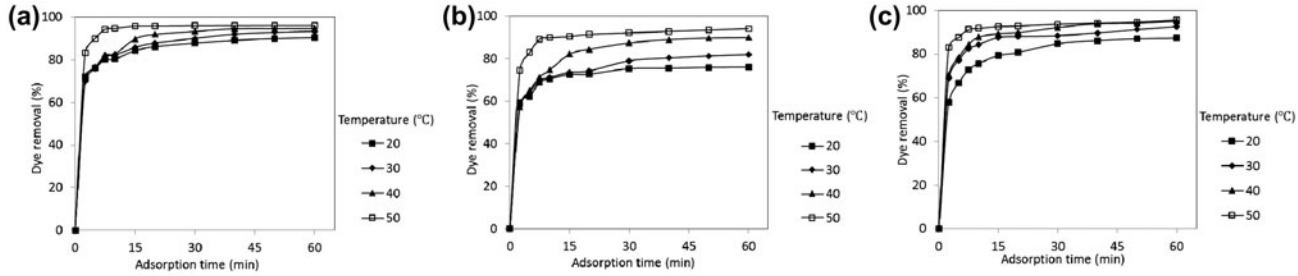

Fig. 10. The effect of temperature on dye removal percent using FCZN: (a) DR23, (b) DR80, and (c) DR81 (adsorbent dosages were 0.15, 0.2, and 0.3 g/L for DR23, DR80, and DR81, respectively, initial concentration = 50 mg/L, pH 2).

adsorbed dye/g adsorbent), the maximum adsorption capacity (mg/g), the equilibrium concentration of dye solution (mg/L), and Langmuir constant (L/mg), respectively. The linear form of Langmuir equation can be expressed by:

$$\frac{C_e}{q_e} = \frac{1}{K_L q_0} + \frac{C_e}{q_0} \tag{2}$$

where q_0, K_L, and coefficient of determination (R^2) were indicated by linear plotting C_e/q_e vs. C_e (Table 3). The essential characteristics of the Langmuir isotherm can be represented by a dimensionless constant called equilibrium parameter, R_L, which is defined by following equation:

$$R_L = \frac{1}{(1 + K_L C_0)} \tag{3}$$

The R_L values indicate the type of isotherm to be irreversible ($R_L = 0$), favorable ($0 < R_L < 1$), linear ($R_L = 1$), or unfavorable ($R_L > 1$) [55,56]. For all three dyes, the values of R_L were in favorable section.

The Freundlich expression is an empirical equation based on adsorption on a heterogeneous surface and it is not limited to the formation of the monolayer [57]. Isotherm data were tested with Freundlich isotherm which can be expressed using the following equation:

$$q_e = K_F C_e^{1/n} \tag{4}$$

Eq. (4) can be rearranged to a linear form:

$$\log q_e = \log K_F + (1/n) \log C_e \tag{5}$$

where K_F and $1/n$ are the adsorption capacity at unit concentration and adsorption intensity, respectively. The values of K_F, $1/n$, and R^2 were determined by using a linear plot of $\log q_e$ vs. $\log C_e$ (Table 3). The latter constant can be classified as irreversible ($1/n = 0$), favorable ($0 < 1/n < 1$), and unfavorable ($1/n > 1$) [58]. As shown in Table 3, the values of $1/n$ are in favorable section for all three dyes.

Tempkin isotherm model describes that the heat of adsorption of all the molecules on the adsorbent surface layer would decrease linearly with coverage due to adsorbate–adsorbate interactions [59]. The Tempkin equation is given as:

$$q_e = (RT/b) \ln(A_T C_e) \tag{6}$$

which can be linearized as follows:

$$q_e = B_T \ln A_T + B_T \ln C_e \tag{7}$$

where

$$B_T = \frac{RT}{b} \tag{8}$$

where B_T and A_T (L/mg) are the Tempkin constant. T and R are the absolute temperature (K) and universal gas constant (8.314 J/mol K), respectively. The constant b is related to heat of adsorption [59]. A_T, B_T, and R^2 were obtained by linear plotting q_e vs. $\ln C_e$ (Table 3).

If each of these three models is applicable, its linear form should give a line with the highest value of R^2. The lines fitted according to these models, using equilibrium data at different adsorbent dosage. Table 3 represents the constant values of isotherms and R^2 values. According to values of R^2, Langmuir isotherm gave the best correlation for the adsorption process in this study because the dye adsorption on FCZN took

Table 3
Isotherm coefficients for adsorption of all three dyes using FCZN at different adsorbent dosages

Langmuir			Freundlich			Tempkin		
q_0	K_L	R^2	K_F	$1/n$	R^2	A_T	B_T	R^2
DR23								
362	0.5287	0.9888	266	0.0681	0.6797	1.2E5	22	0.6559
DR80								
208	1.5484	0.9979	190	0.015	0.5170	1.2E28	3	0.5088
DR81								
160	1.3021	0.9998	135	0.0419	0.9811	1.5E9	6	0.981

place at specific homogeneous sites and a one layer adsorption was formed.

3.4. Adsorption kinetic

It is necessary to evaluate the kinetic to provide information about the rate of adsorption onto the adsorbent. The evaluation of kinetic was done by applying pseudo-first-order, pseudo-second-order, and intraparticle diffusion model [60,61].

Linear form of pseudo-first-order model is illustrated as:

$$\log(q_e - q_t) = \log(q_e) - \left(\frac{k_1}{2.303}\right)t \tag{9}$$

where q_e, q_t, and k_1 are the amount of dye adsorbed onto the adsorbent at equilibrium (mg adsorbed dye/g adsorbent), the amount of adsorbed dye at time t (mg/g), and the equilibrium rate constant of pseudo-first-order kinetic (1/min), respectively.

A linear form of pseudo-second-order equation is:

$$\frac{t}{q_t} = \frac{1}{k_2 q_e^2} + \frac{1}{q_e}t \tag{10}$$

where k_2 is the equilibrium rate constant of pseudo-second-order kinetic (g/mg min).

The equation of intraparticle diffusion model is given as:

$$q_t = k_p t^{1/2} + I \tag{11}$$

where k_p and I are the intraparticle diffusion rate constant and intercept, respectively.

Using the data obtained from the evaluation of the effect of initial dye concentration, $\log(q_e - q_t)$ vs. t, t/q_t vs. t, and q_t vs. $t^{1/2}$ were plotted. As a result, Table 4 represents the linearized kinetic parameters for dye adsorption using FCZN. By comparing the values of R^2, it was observed that the pseudo-second-order kinetic could best describe adsorption kinetic.

3.5. Adsorption thermodynamic

Thermodynamic can express direction (spontaneous reaction or its reverse) and type (exothermic or endothermic and physical or chemical) of reactions. Thermodynamic parameters can be obtained using the following equations [62]:

$$K_C = C_A/C_S \tag{12}$$

$$\ln K_C = (\Delta S/R) - (\Delta H/RT) \tag{13}$$

$$\Delta G = \Delta H - T\Delta S \tag{14}$$

where K_C, C_A, C_S, ΔS, ΔH, R, T, and ΔG are the equilibrium constant, the amount of dye adsorbed on the adsorbent of the solution at equilibrium (mol/L), the equilibrium concentration of dye in the solution (mol/L), entropy (kJ/mol K), enthalpy (kJ/mol), the gas constant (8.314 J/mol K), absolute temperature (K), and Gibbs free energy (kJ/mol), respectively.

A linear curve of $\ln K_C$ vs. $1/T$ was plotted for each dye and the values of ΔS and ΔH were calculated by using the values of the slope and intercept. Also, the values of ΔG were calculated by Eq. (14) for all temperatures. Table 5 presents the values of thermodynamic parameters of dye adsorption process.

Table 4
Linearized kinetic parameters for dye adsorption using FCZN at different initial dye concentrations

Dye (mg/L)	Pseudo-first-order				Pseudo-second-order			Intraparticle diffusion		
	$(q_e)_{exp}$	$(q_e)_{cal}$	k_1	R^2	$(q_e)_{cal}$	k_2	R^2	k_p	I	R^2
DR23										
50	301	95	0.0845	0.9100	303	0.0029	0.9999	9	236	0.8964
100	354	140	0.0873	0.9361	357	0.0019	0.9996	13	260	0.9237
150	372	131	0.05642	0.8315	370	0.0015	0.999	15	261	0.9442
200	403	166	0.0861	0.9459	417	0.0014	0.9998	18	282	0.8874
DR80										
50	191	41	0.1306	0.8973	192	0.0097	0.9999	5	160	0.5533
100	245	94	0.0668	0.8747	250	0.0022	0.9992	10	171	0.9111
150	252	121	0.0684	0.9106	256	0.0016	0.9993	15	149	0.8783
200	279	113	0.06218	0.8787	286	0.0016	0.9994	14	178	0.8386
DR81										
50	145	70	0.0981	0.9602	149	0.0037	0.9999	7	98	0.8450
100	155	98	0.1172	0.9608	161	0.0029	0.9996	8	99	0.8590
150	160	68	0.0721	0.8907	164	0.0031	0.9993	7	108	0.8902
200	163	72	0.0705	0.8778	167	0.0028	0.9977	7	110	0.9138

Table 5
Values of thermodynamic parameters of dye adsorption process

Dye	T (°C)	Thermodynamic parameters			R^2
		ΔG_0 (kJ/mol)	ΔH_0 (kJ/mol)	ΔS_0 (kJ/mol)	
DR23	20	−5.5005	24.8131	0.1035	0.9914
	30	−6.5351			
	40	−7.5697			
	50	−8.6043			
DR80	20	−2.5880	43.1821	0.1562	0.9804
	30	−4.1501			
	40	−5.7122			
	50	−7.2743			
DR81	20	−4.9183	30.7643	0.1218	0.9421
	30	−6.1361			
	40	−7.3539			
	50	−8.5718			

The positive values of ΔS suggest increased randomness at the solid/solution interface occurs in the internal structure of the adsorption of dye onto FCZN. The positive values of ΔH indicate the presence of an energy barrier in the adsorption process and endothermic process. Also, the negative values of ΔG express that the adsorption process is spontaneous [63]. The change in Gibbs free energy for physical and chemical adsorption are between −20 and 0 kJ/mol and −80 and −400 kJ/mol, respectively [64]. Based on the obtained values of ΔG, physisorption was the dominant mechanism in this study.

3.6. Desorption studies

The adsorbent regeneration is an important factor for economic treatment process. Desorption studies are useful to recover the dye and the adsorbent. Dye desorption tests showed that the maximum dye release of 84% for DR23, 89% for DR80, and 81% for

DR81 were achieved in aqueous solution at pH 12. At higher pH value, the number of positively charged sites decreases which favors adsorbent regeneration.

3.7. Genetic programming

Genetic algorithm (GA) imitates biological evolution and progressively seeks superior solutions for an optimization problem using the guide of selective function (fitness) and partial combination of candidate solutions [65,66]. GP was introduced as an extension of GA by Koza [67] which produces computer programs or models for solving regression problems, using the principle of Darwinian natural selection [68]. GP acts based on GA, with a difference that GA provides solutions in form of a string of numbers, while GP presents solutions by computer programs. The programs include tree structures with their nodes (functions) and terminals (leaves) [67–69]. In this study, based on experimental data, GP was applied to produce an optimal formula in which the error is minimum.

Fig. 11 illustrates flowchart of proposed GP. At first, initial population of programs is generated randomly, and then the fitness values are calculated for all programs. In this study, sum of absolute differences between experimental and predicted values is considered as fitness value. Furthermore, if a specific criterion (in this investigation the maximum number of generations) is met, the algorithm is stopped and the program with the best fitness is presented; otherwise, new generation of programs are generated by selecting parents based on their fitness and breeding them via genetic operators such as crossover, mutation and reproduction [69]. In the next step, after calculating fitness values, termination criteria should be checked. The process of generating new programs continues until the termination criterion is reached.

The genetic operators should be applied in a suitable way in order to produce better generation. The operators can be defined as follows [70]: (i) The crossover operator exchanges sub-trees between a pair of tree structure programs (parents), and two offsprings are generated from them. (ii) The mutation operator substitutes a randomly selected sub-tree of a program with new sub-tree which is generated randomly. (iii) The reproduction operator copies the best programs in the next generation.

The performance of modeling was statistically evaluated by the coefficient of determination (R^2) using the following equation:

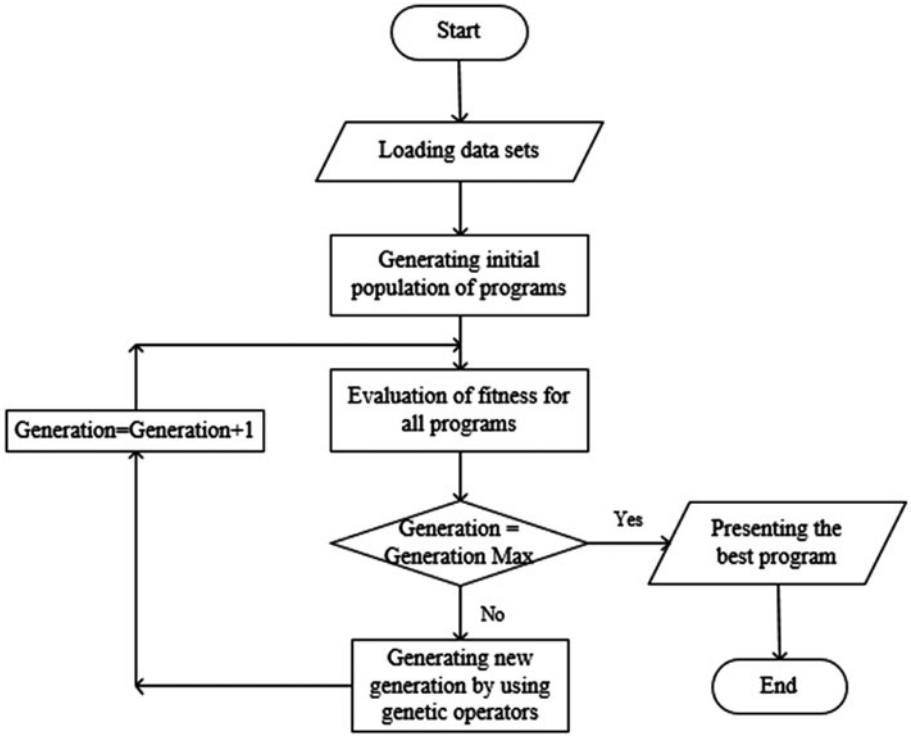

Fig. 11. Flowchart of proposed GP.

$$R^2 = 1 - \frac{\sum_{i=1}^{N} (y_{i,\text{pred}} - y_{i,\text{exp}})^2}{\sum_{i=1}^{N} (y_{i,\text{exp}} - \bar{y}_{\text{exp}})^2} \quad (15)$$

where N is the number of data points, $y_{i,\text{pred}}$ and $y_{i,\text{exp}}$ are the predicted and experimental y value of point i, respectively, and $\bar{y}_{\text{exp}}$ is the average of experimental values.

In this study, GP was used for adsorption process modeling. At first, in order to have similar domains, all input and output variables were normalized between 0.1 and 0.9. The modeling was done in MATLAB R2009a environment. Table 6 illustrates the ranges of experimental data. Based on presented flowchart (Fig. 11), modeling was performed by using training data-sets (90% of all data-sets) and the obtained equations were tested with testing data-sets (10% of all data-sets). The training and testing data-sets were chosen randomly. In this modeling, the function set that were used included elements such as: +, −, ×, sin, cos, log, and abs. Eqs. (16)–(18) present the GP models obtained for DR23, DR80, and DR81, respectively.

$$\begin{aligned} Y = {} & \sin(((\log(\text{abs}(\cos((\cos((((((x_4 \times (\log(\text{abs}(\cos(x_5))) \\ & + (x_3 - \log(x_2)))) \times ((((((\cos(x_3) + x_1) \times x_5) \\ & \times \cos(x_3)) - x_2) - x_2)) - x_2) - \cos((((\cos(\cos(\log(x_4) \\ & \times x_1)) + \sin(-x_2 - x_4)) \\ & \times \sin(((\log(\text{abs}(\cos((\cos((((((\cos(x_3) + x_1) \times x_5) \\ & \times \cos(x_3)) - x_2) - \cos(2x_4 + x_3))) \times (\cos(\cos(2x_3)) \\ & + \sin(\sin(x_2 - 3x_4)))))))) - x_2) \times \log(\text{abs}(\sin(x_2)))))) \\ & + x_3)))) \times (\cos(\cos(2x_3)) + \sin(\sin(-2x_4)))))))) - x_2) \\ & \times \log(\text{abs}(\sin(\sin(x_2)))))) \end{aligned} \quad (16)$$

$$\begin{aligned} Y = {} & \cos(\cos(\sin(\cos(\cos(\sin(x_5)))) - (\sin(\cos(x_5)) \\ & \times (\sin((x_1 \times x_3) + (\cos(x_2) + x_3)) \\ & \times (\sin(\cos(\cos(\sin(x_5)))) \times ((((x_1 \\ & \times \sin(\cos(\log(\text{abs}(3x_1 + x_5 - x_3))))) - \sin(\sin(x_2))) \\ & \times x_5) + x_4))))))) - (\sin(\sin(\cos((\cos(\cos(x_3 + x_1)) \\ & - (\sin((x_4 + \cos(((\log(x_2 + x_4) - x_5) + \cos(x_2)) \\ & \times x_5))) \times x_4)) \times (x_3 - \log(x_2 + x_4))))) \times (\cos(\sin(x_1)) \\ & \times \sin(\cos(\cos(\cos(x_3 + (\cos(\cos(\cos(x_5))) \\ & - (\sin(\sin(\sin(\cos(\cos(x_5)) + \log(x_4)))) \times x_4)))))))) \end{aligned} \quad (17)$$

$$\begin{aligned} Y = {} & ((\log(\text{abs}(\cos(x_2))) \times x_3) + \sin(\sin(\sin(((x_5 - \log(x_5)) \\ & + (((x_3 \times (((\cos(x_4) \times \cos(x_4)) - (x_4 - x_3)) \\ & - \sin((((x_3 \times ((x_2 - x_5) - x_4)) - \log(x_5)) + \cos(x_5 \\ & - \log(x_3))) \times ((x_4 \times \log(x_4)) - (\sin(x_2) \times (x_1 \\ & \times \log(x_2))))))) \times (x_1 - x_3)) + x_5)) \times x_5)) - (x_4 \\ & - x_3))) \times \cos(\cos(\sin((x_1 \times ((x_4 \times (x_4 \times x_3)) \\ & + \cos(x_3))) \times (((\log(\text{abs}(\cos(x_2))) \times x_3) \\ & + \sin((\sin(\cos(\sin(x_5 - \log(x_5)))) \times x_4) - (x_4 - x_3))) \\ & \times (x_3 \times x_4))) - \log(\text{abs}(\log(\text{abs}((x_2 - \sin(x_4)) \\ & \times \cos(x_2))))))) \end{aligned} \quad (18)$$

where x_1, x_2, x_3, x_4, x_5, and Y are normalized values of contact time, initial dye concentration, adsorbent dosage, pH, temperature, and dye removal percent, respectively.

As it can be seen in Fig. 12, both training and testing data-sets are well distributed in a narrow area around the diagonal line. In other words, the predicted and experimental dye removal percents have similar values to a large extent. Moreover, the calculated values of R^2 confirm the reliability of the GP modeling for adsorption process.

Table 6
Ranges of experimental data

	Ranges		
Variable	DR23	DR80	DR81
Input			
Adsorption time (min)	2.5–60	2.5–60	2.5–60
Initial dye concentration (mg/L)	50–200	50–200	50–200
Adsorbent dosage (g/L)	0.025–0.15	0.08–0.26	0.05–0.3
pH	2–10	2–10	2–10
Temperature (˚C)	20–50	20–50	20–50
Output			
Dye removal percent (%)	0–100	0–100	0–100

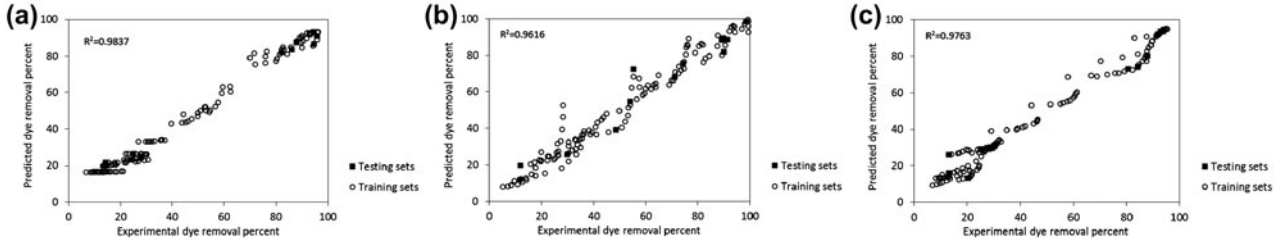

Fig. 12. Comparison of predicted dye removal percent resulted from GP with experimental values for: (a) DR23, (b) DR80, and (c) DR81.

4. Conclusion

In this research, CZN was synthesized and 3-aminopropyltrimethoxysilane was used to functionalize CZN. The synthesized materials were characterized using FTIR, SEM, XRD, XRF, and BET. Equilibrium and kinetic data were fitted by Langmuir isotherm and pseudo-second-order kinetic, respectively. The thermodynamic data showed that dye adsorption was a spontaneous, endothermic, and physical reaction. The results indicate that FCZN can be used as a suitable adsorbent for dye removal from colored wastewater. On the other hand, an important advantage of GP modeling is to present an explicit equation. In addition, lack of need to conceptual design is another positive point of this kind of modeling. Based on these advantages and the obtained results, GP is recommended as a suitable tool for modeling of dye adsorption process.

Acknowledgment

This work was done in Department of Environmental Research, Institute for Color Science and Technology. Professor Mahmoodi is grateful for the support from the ICST.

References

[1] M. Ghaedi, M. Ghayedi, S.N. Kokhdan, R. Sahraei, A. Daneshfar, Palladium, silver, and zinc oxide nanoparticles loaded on activated carbon as adsorbent for removal of bromophenol red from aqueous solution, J. Ind. Eng. Chem. 19 (2013) 1209–1217.
[2] E.N. El Qada, S.J. Allen, G.M. Walker, Adsorption of basic dyes from aqueous solution onto activated carbons, Chem. Eng. J. 135 (2008) 174–184.
[3] N.M. Mahmoodi, N.Y. Limaee, M. Arami, S. Borhany, M. Mohammad-Taheri, Nanophotocatalysis using nanoparticles of titania: Mineralization and finite element modelling of Solophenyl dye decolorization, J. Photochem. Photobiol., A: Chem. 189 (2007) 1–6.
[4] M. Roosta, M. Ghaedi, A. Daneshfar, R. Sahraei, A. Asghari, Optimization of the ultrasonic assisted removal of methylene blue by gold nanoparticles loaded on activated carbon using experimental design methodology, Ultrason. Sonochem. 21 (2014) 242–252.
[5] A. Hassani, F. Vafaei, S. Karaca, A. Khataee, Adsorption of a cationic dye from aqueous solution using Turkish lignite: Kinetic, isotherm, thermodynamic studies and neural network modeling, J. Ind. Eng. Chem. 20 (2014) 2615–2624.
[6] N.M. Mahmoodi, Surface modification of magnetic nanoparticle and dye removal from ternary systems, J. Ind. Eng. Chem. 27 (2015) 251–259.
[7] M. Yalili Kilic, T. Yonar, S. Teker, K. Kestioğlu, Comparing treatment methods that remove color from the effluent of an organized industrial district (OID), Desalin. Water Treat. 54 (2015) 3454–3463.
[8] N.M. Mahmoodi, Photodegradation of dyes using multiwalled carbon nanotube and ferrous ion, J. Environ. Eng. 139 (2013) 1368–1374.
[9] N.M. Mahmoodi, Zinc ferrite nanoparticle as a magnetic catalyst: Synthesis and dye degradation, Mater. Res. Bull. 48 (2013) 4255–4260.
[10] N.M. Mahmoodi, Photocatalytic ozonation of dyes using multiwalled carbon nanotube, J. Mol. Catal. A: Chem. 366 (2013) 254–260.
[11] N.M. Mahmoodi, B. Hayati, M. Arami, H. Bahrami, Preparation, characterization and dye adsorption properties of biocompatible composite, (alginate/titania nanoparticle), Desalination 275 (2011) 93–101.
[12] N.M. Mahmoodi, Manganese ferrite nanoparticle: Synthesis, characterization and photocatalytic dye degradation ability, Desalin. Water Treat. 53 (2015) 84–90.
[13] N.M. Mahmoodi, Synthesis of amine-functionalized magnetic ferrite nanoparticle and its dye removal ability, J. Environ. Eng. 139 (2013) 1382–1390.
[14] N.M. Mahmoodi, M. Arami, H. Bahrami, S. Khorramfar, Novel biosorbent (Canola hull): Surface characterization and dye removal ability at different cationic dye concentrations, Desalination 264 (2010) 134–142.
[15] G. Crini, P.-M. Badot, Application of chitosan, a natural aminopolysaccharide, for dye removal from aqueous solutions by adsorption processes using batch studies: A review of recent literature, Prog. Polym. Sci. 33 (2008) 399–447.
[16] M. Roosta, M. Ghaedi, A. Daneshfar, R. Sahraei, Experimental design based response surface methodology optimization of ultrasonic assisted

adsorption of safaranin O by tin sulfide nanoparticle loaded on activated carbon, Spectrochim. Acta Part A Mol. Biomol. Spectrosc. 122 (2014) 223–231.
[17] Y.-S. Ho, G. Mckay, Kinetic models for the sorption of dye from aqueous solution by wood, Process Saf. Environ. Prot. 76 (1998) 183–191.
[18] L. Morais, O. Freitas, E. Gonçalves, L. Vasconcelos, C. González Beça, Reactive dyes removal from wastewaters by adsorption on eucalyptus bark: Variables that define the process, Water Res. 33 (1999) 979–988.
[19] C. Namasivayam, D. Arasi, Removal of congo red from wastewater by adsorption onto waste red mud, Chemosphere 34 (1997) 401–417.
[20] O. Ozdemir, B. Armagan, M. Turan, M.S. Çelik, Comparison of the adsorption characteristics of azo-reactive dyes on mezoporous minerals, Dyes Pigm. 62 (2004) 49–60.
[21] M. Özacar, I.A. Şengil, Adsorption of reactive dyes on calcined alunite from aqueous solutions, J. Hazard. Mater. 98 (2003) 211–224.
[22] Z. Chen, J. Zhang, J. Fu, M. Wang, X. Wang, R. Han, Q. Xu, Adsorption of methylene blue onto poly(cyclotriphosphazene-co-4,4´-sulfonyldiphenol) nanotubes: Kinetics, isotherm and thermodynamics analysis, J. Hazard. Mater. 273 (2014) 263–271.
[23] M. Ghaedi, S. Heidarpour, S. Nasiri Kokhdan, R. Sahraie, A. Daneshfar, B. Brazesh, Comparison of silver and palladium nanoparticles loaded on activated carbon for efficient removal of Methylene blue: Kinetic and isotherm study of removal process, Powder Technol. 228 (2012) 18–25.
[24] E.H.C. Kaewprasit, N. Abidi, J.P. Gourlot, Application of methylene blue adsorption to cotton fiber specific surface area measurement: Part 1. Methodology, J. Cotton Sci. 2 (1998) 164–173.
[25] Y. Yao, S. Miao, S. Liu, L.P. Ma, H. Sun, S. Wang, Synthesis, characterization, and adsorption properties of magnetic Fe_3O_4@graphene nanocomposite, Chem. Eng. J. 184 (2012) 326–332.
[26] R. Wu, J. Qu, Y. Chen, Magnetic powder MnO–Fe_2O_3 composite—A novel material for the removal of azo-dye from water, Water Res. 39 (2005) 630–638.
[27] G. Moussavi, M. Mahmoudi, Removal of azo and anthraquinone reactive dyes from industrial wastewaters using MgO nanoparticles, J. Hazard. Mater. 168 (2009) 806–812.
[28] B. Cheng, Y. Le, W. Cai, J. Yu, Synthesis of hierarchical $Ni(OH)_2$ and NiO nanosheets and their adsorption kinetics and isotherms to Congo red in water, J. Hazard. Mater. 185 (2011) 889–897.
[29] S. Qadri, A. Ganoe, Y. Haik, Removal and recovery of acridine orange from solutions by use of magnetic nanoparticles, J. Hazard. Mater. 169 (2009) 318–323.
[30] Z. Zhang, J. Kong, Novel magnetic Fe_3O_4@C nanoparticles as adsorbents for removal of organic dyes from aqueous solution, J. Hazard. Mater. 193 (2011) 325–329.
[31] M. Ghaedi, A. Ansari, M. Habibi, A. Asghari, Removal of malachite green from aqueous solution by zinc oxide nanoparticle loaded on activated carbon: Kinetics and isotherm study, J. Ind. Eng. Chem. 20 (2014) 17–28.
[32] M. Iram, C. Guo, Y. Guan, A. Ishfaq, H. Liu, Adsorption and magnetic removal of neutral red dye from aqueous solution using Fe_3O_4 hollow nanospheres, J. Hazard. Mater. 181 (2010) 1039–1050.
[33] M. Maghsoudi, M. Ghaedi, A. Zinali, A. Ghaedi, M. Habibi, Artificial neural network (ANN) method for modeling of sunset yellow dye adsorption using zinc oxide nanorods loaded on activated carbon: Kinetic and isotherm study, Spectrochim. Acta Part A Mol. Biomol. Spectrosc. 134 (2015) 1–9.
[34] M. Ghaedi, A. Daneshfar, A. Ahmadi, M. Momeni, Artificial neural network-genetic algorithm based optimization for the adsorption of phenol red (PR) onto gold and titanium dioxide nanoparticles loaded on activated carbon, J. Ind. Eng. Chem. 21 (2015) 587–598.
[35] R. Aghav, S. Kumar, S. Mukherjee, Artificial neural network modeling in competitive adsorption of phenol and resorcinol from water environment using some carbonaceous adsorbents, J. Hazard. Mater. 188 (2011) 67–77.
[36] A.H. Gandomi, A.H. Alavi, S. Kazemi, M. Gandomi, Formulation of shear strength of slender RC beams using gene expression programming, part I: Without shear reinforcement, Autom. Constr. 42 (2014) 112–121.
[37] D. Bingöl, M. Inal, S. Çetintaş, Evaluation of copper biosorption onto date palm (*Phoenix dactylifera* L.) seeds with MLR and ANFIS models, Ind. Eng. Chem. Res. 52 (2013) 4429–4435.
[38] M.J. Amiri, J. Abedi-Koupai, S.S. Eslamian, S.F. Mousavi, H. Hasheminejad, Modeling Pb(II) adsorption from aqueous solution by ostrich bone ash using adaptive neural-based fuzzy inference system, J. Environ. Sci. Health, Part A 48 (2013) 543–558.
[39] M. Ghaedi, R. Hosaininia, A. Ghaedi, A. Vafaei, F. Taghizadeh, Adaptive neuro-fuzzy inference system model for adsorption of 1,3,4-thiadiazole-2,5-dithiol onto gold nanoparticales-activated carbon, Spectrochim. Acta Part A Mol. Biomol. Spectrosc. 131 (2014) 606–614.
[40] M. Ghaedi, A. Ghaedi, F. Abdi, M. Roosta, A. Vafaei, A. Asghari, Principal component analysis-adaptive neuro-fuzzy inference system modeling and genetic algorithm optimization of adsorption of methylene blue by activated carbon derived from Pistacia khinjuk, Ecotoxicol. Environ. Saf. 96 (2013) 110–117.
[41] N.M. Mahmoodi, M. Arabloo, J. Abdi, Laccase immobilized manganese ferrite nanoparticle: Synthesis and LSSVM intelligent modeling of decolorization, Water Res. 67 (2014) 216–226.
[42] M. Ghaedi, A. Ghaedi, M. Hossainpour, A. Ansari, M. Habibi, A. Asghari, Least square-support vector (LS-SVM) method for modeling of methylene blue dye adsorption using copper oxide loaded on activated carbon: Kinetic and isotherm study, J. Ind. Eng. Chem. 20 (2014) 1641–1649.
[43] B. Li, Y. Wang, Facile synthesis and photocatalytic activity of ZnO–CuO nanocomposite, Superlattices Microstruct. 47 (2010) 615–623.
[44] N. Sobana, K. Selvam, M. Swaminathan, Optimization of photocatalytic degradation conditions of Direct Red 23 using nano-Ag doped TiO_2, Sep. Purif. Technol. 62 (2008) 648–653.
[45] H. Kusic, N. Koprivanac, L. Srsan, Azo dye degradation using Fenton type processes assisted by UV

irradiation: A kinetic study, J. Photochem. Photobiol., A 181 (2006) 195–202.
[46] N.M. Mahmoodi, S. Khorramfar, F. Najafi, Amine-functionalized silica nanoparticle: Preparation, characterization and anionic dye removal ability, Desalination 279 (2011) 61–68.
[47] B. Nandi, A. Goswami, M. Purkait, Adsorption characteristics of brilliant green dye on kaolin, J. Hazard. Mater. 161 (2009) 387–395.
[48] G.M.L.D.L. Pavia, G.S. Kaiz, Introduction to Spectroscopy: A Guide for Students of Organic Chemistry, W.B. Saunders Company, Philadelphia, 1987.
[49] N.M. Mahmoodi, Synthesis of core–shell magnetic adsorbent nanoparticle and selectivity analysis for binary system dye removal, J. Ind. Eng. Chem. 20 (2014) 2050–2058.
[50] G. Crini, F. Gimbert, C. Robert, B. Martel, O. Adam, N. Morin-Crini, F. De Giorgi, P.M. Badot, The removal of Basic Blue 3 from aqueous solutions by chitosan-based adsorbent: Batch studies, J. Hazard. Mater. 153 (2008) 96–106.
[51] N.M. Mahmoodi, J. Abdi, F. Najafi, Synthesis of urethane polycarboxylate as a novel adsorbent and its binary system dye removal ability from aqueous solution, Fibers Polym. 15 (2014) 446–456.
[52] C. Moreno-Castilla, Adsorption of organic molecules from aqueous solutions on carbon materials, Carbon 42 (2004) 83–94.
[53] M. Ghaedi, A.G. Nasab, S. Khodadoust, R. Sahraei, A. Daneshfar, Characterization of zinc oxide nanorods loaded on activated carbon as cheap and efficient adsorbent for removal of methylene blue, J. Ind. Eng. Chem. 21 (2015) 986–993.
[54] M. Alkan, M. Doğan, Y. Turhan, Ö. Demirbaş, P. Turan, Adsorption kinetics and mechanism of maxilon blue 5G dye on sepiolite from aqueous solutions, Chem. Eng. J. 139 (2008) 213–223.
[55] M. Greluk, Z. Hubicki, Kinetics, isotherm and thermodynamic studies of Reactive Black 5 removal by acid acrylic resins, Chem. Eng. J. 162 (2010) 919–926.
[56] X. Wu, D. Wu, R. Fu, Studies on the adsorption of reactive brilliant red X-3B dye on organic and carbon aerogels, J. Hazard. Mater. 147 (2007) 1028–1036.
[57] A. Özcan, A.S. Özcan, Adsorption of Acid Red 57 from aqueous solutions onto surfactant-modified sepiolite, J. Hazard. Mater. 125 (2005) 252–259.
[58] M. Greluk, Z. Hubicki, Sorption of SPADNS azo dye on polystyrene anion exchangers: Equilibrium and kinetic studies, J. Hazard. Mater. 172 (2009) 289–297.
[59] A. Nemr, Potential of pomegranate husk carbon for Cr(VI) removal from wastewater: Kinetic and isotherm studies, J. Hazard. Mater. 161 (2009) 132–141.
[60] S. Senthilkumaar, P. Kalaamani, K. Porkodi, P. Varadarajan, C. Subburaam, Adsorption of dissolved reactive red dye from aqueous phase onto activated carbon prepared from agricultural waste, Bioresour. Technol. 97 (2006) 1618–1625.
[61] W. Weber, J. Morris, Kinetics of adsorption on carbon from solution, J. Sanit. Eng. Div. Am. Soc. Civ. Eng. 89 (1963) 31–60.
[62] A. Özcan, E.M. Öncü, A.S. Özcan, Kinetics, isotherm and thermodynamic studies of adsorption of Acid Blue 193 from aqueous solutions onto natural sepiolite, Colloids Surf., A 277 (2006) 90–97.
[63] G.M. Barrow, Physical Chemistry, fifth ed., Mc Graw—Hill, New York, 1988.
[64] M.J. Jaycock, G.D. Parfitt, Chemistry of Interfaces, Halstead Press, John Wiley and Sons, New York, 1981.
[65] Y. Yang, G. Wang, B. Wang, Z. Li, X. Jia, Q. Zhou, et al., Biosorption of Acid Black 172 and Congo Red from aqueous solution by nonviable Penicillium YW 01: Kinetic study, equilibrium isotherm and artificial neural network modeling, Bioresour. Technol. 102 (2011) 828–834.
[66] M. Ooba, T. Hirano, J.-I. Mogami, R. Hirata, Y. Fujinuma, Comparisons of gap-filling methods for carbon flux dataset: A combination of a genetic algorithm and an artificial neural network, Ecol. Model. 198 (2006) 473–486.
[67] J.R. Koza, Genetic Programming: On the Programming of Computers by Means of Natural Selection, MIT press, Cambridge, MA, 1992.
[68] A. Garg, V. Vijayaraghavan, S. Mahapatra, K. Tai, C. Wong, Performance evaluation of microbial fuel cell by artificial intelligence methods, Expert Syst. Appl. 41 (2014) 1389–1399.
[69] A. Fouladitajar, F.Z. Ashtiani, A. Okhovat, B. Dabir, Membrane fouling in microfiltration of oil-in-water emulsions; a comparison between constant pressure blocking laws and genetic programming (GP) model, Desalination 329 (2013) 41–49.
[70] A. Okhovat, S.M. Mousavi, Modeling of arsenic, chromium and cadmium removal by nanofiltration process using genetic programming, Appl. Soft Comput. 12 (2012) 793–799.